AIP Journal of Applied Physics

Phenomenological scattering-rate model for the simulation of the current density and emission power in mid-infrared quantum cascade lasers

S. S. Kurlov, Y. V. Flores, M. Elagin, M. P. Semtsiv, L. Schrottke, H. T. Grahn, G. G. Tarasov, and W. T. Masselink

Citation: Journal of Applied Physics **119**, 134501 (2016); doi: 10.1063/1.4945364
View online: http://dx.doi.org/10.1063/1.4945364
View Table of Contents: http://scitation.aip.org/content/aip/journal/jap/119/13?ver=pdfcov
Published by the AIP Publishing

Phenomenological scattering-rate model for the simulation of the current density and emission power in mid-infrared quantum cascade lasers

S. S. Kurlov,[1,2] Y. V. Flores,[1] M. Elagin,[1] M. P. Semtsiv,[1] L. Schrottke,[3] H. T. Grahn,[3] G. G. Tarasov,[2] and W. T. Masselink[1]
[1]*Department of Physics, Humboldt-Universität zu Berlin, Newtonstraße 15, 12489 Berlin, Germany*
[2]*Institute of Semiconductor Physics, National Academy of Sciences, pr. Nauki 45, Kiev-03028, Ukraine*
[3]*Paul-Drude-Institut für Festkörperelektronik, Hausvogteiplatz 5–7, 10117 Berlin, Germany*

(Received 17 December 2015; accepted 22 March 2016; published online 1 April 2016)

A phenomenological scattering-rate model introduced for terahertz quantum cascade lasers (QCLs) [Schrottke *et al*., Semicond. Sci. Technol. **25**, 045025 (2010)] is extended to mid-infrared (MIR) QCLs by including the energy dependence of the intersubband scattering rates for energies higher than the longitudinal optical phonon energy. This energy dependence is obtained from a phenomenological fit of the intersubband scattering rates based on published lifetimes of a number of MIR QCLs. In our approach, the total intersubband scattering rate is written as the product of the exchange integral for the squared moduli of the envelope functions and a phenomenological factor that depends only on the transition energy. Using the model to calculate scattering rates and imposing periodical boundary conditions on the current density, we find a good agreement with low-temperature data for current-voltage, power-current, and energy-photon flux characteristics for a QCL emitting at 5.2 μm.
 [http://dx.doi.org/10.1063/1.4945364]

I. INTRODUCTION

Since their invention in 1994,[1] quantum cascade lasers (QCLs) have become the standard semiconductor laser source for the mid- and far-infrared spectral range. These unipolar devices are based on the population inversion between quantized subbands in biased semiconductor heterostructures. After undergoing an intersubband transition, the electron remains within the conduction band and thus can be injected into the next intersubband emission stage. The emission stages are cascaded one after another, thus allowing many photons to be emitted by a single electron. QCLs achieving large peak powers (6–14 W), power efficiencies (15%–35%), and transition efficiencies (up to 90%) have been reported for the mid-infrared (MIR) spectral region for temperatures between 80 and 300 K.[2–5] These high powers and high efficiencies, together with the possibility of single-mode emission[6] and wavefront engineering,[7] make QCLs to be very attractive for several applications including gas sensing, optical spectroscopy, and infrared countermeasures.[8,9]

A useful theoretical model is essential for the optimization and further development of new QCL sources. Such a model is expected to significantly reduce the experimental effort of QCL optimization for a given wavelength. It requires the calculation of the subband structure including its bias dependence and the location of charge as well as the non-parabolicity of the band structure, scattering effects, and the optical mode confinement. *Ab initio* models are characterized by their intricacy and the relatively complex formulation of the different scattering mechanisms.[10–12] Calculations made by *ab initio* models lead to good agreement between theory and experiment, yet at high computational costs.

In this work, we propose a bottom-up approach, which consists of using experimental results and describing them with a phenomenological model. Such a scattering-rate model has been recently developed for terahertz (THz) QCLs.[13] In this approach, several non-radiative scattering mechanisms including scattering via optical and acoustic phonons, electron-electron interaction, and scattering at ionized impurities are written in terms of the squared modulus of the dipole matrix element $|Z_{ij}|^2$, which is calculated for intersubband radiative transitions, and a function $f(E_{ij})$ that only depends on the transition energy E_{ij}. The total scattering rate between subbands i and j is given by $f(E_{ij})|Z_{ij}|^2$. Such a description has the advantage of including several scattering mechanisms in a compact form, allowing a straightforward modeling of charge carrier transport. Furthermore, the strategy uses measured data, ensuring accuracy at least within some range of application. The approach was demonstrated using a number of THz QCL designs that were modeled; very good agreement with experimental results in terms of current-voltage characteristics and gain spectra were reported.[13,14]

In case of THz QCLs, the role of scattering of electrons with longitudinal optical (LO) phonons is reduced due to the much larger LO phonon energy (E_{LO}) relative to the radiative transition energy. Therefore, the energy dependent factor $f(E_{ij})$ is taken to be constant for the range of energies of the order of E_{LO} and above, which is a reasonable assumption for THz QCLs.

Furthermore, the assumption of a constant $f(E_{ij})$ for $E_{ij} > E_{LO}$ cannot be applied to MIR QCLs, where intersubband spacing energies are significantly larger than E_{LO}. Therefore, and in contrast to THz QCLs, electron-phonon-interaction plays now a crucial role in electron transport.[15–17] As we show in this work, a more accurate way to describe the total non-radiative scattering rate is to write it in terms of the exchange integral of the envelope functions moduli squared, instead of the dipol matrix element.

The resulting proportionality factor between the exchange integral and the total non-radiative scattering rate (denoted by $\rho(E_{ij})$) is obtained from a phenomenological fit of MIR QCLs lifetimes reported in the literature. This phenomenological fit consists of two parts. The low-energy ($E_{ij} < E_{\mathrm{LO}}$) part has the functional form described in Ref. 13 and parametrizes the contributions arising from several non-radiative scattering mechanisms including electron-electron and interface-roughness scattering. The high-energy ($E_{ij} > E_{\mathrm{LO}}$) tail of the function $\rho(E_{ij})$ has a characteristic decay behavior with increasing intersubband spacing energy, which—as we describe in detail in Section II—is closely related to a reduced electron-phonon scattering rate.

Integrating both parts and fitting lifetimes data for MIR QCLs, the resulting function $\rho(E_{ij})$ becomes suitable for the simulation of MIR QCLs. Once the exchange terms for all transitions have been calculated, the simulation becomes significantly less onerous than including scattering mechanisms separately. We further apply our approach and simulate the performance of an MIR QCL emitting at 5.2 μm at a temperature of 80 K. First results show a satisfactory agreement between the calculated and experimental characteristics.

II. SCATTERING MODEL

QCLs are *n* type semiconductor devices which are typically based on the direct band gap semiconductors. The electron transitions between the states in QCLs are caused mainly by elastic (alloy, interface roughness (IFR), and impurity), inelastic (acoustic and LO phonons), and electron-electron scattering.[18] Electron-electron scattering plays an important role only in the thermalization of the electron distribution within one period of the MIR QCLs.[19] The transverse optical phonon scattering is negligible at the Γ-point of the conduction band due to its spherical symmetry.[20,21] Alloy[22] and acoustic phonon scattering[23] can be approximated by a linear dependence on the wave function overlap ζ

$$\zeta_{ij} = \int dz\, |\psi_i(z)|^2 |\psi_j(z)|^2, \tag{1}$$

for the *i*th and *j*th bound states. However, these scattering effects typically play a secondary role in QCLs. At low temperatures, the electron transport is driven by phonon emission and temperature-independent processes as IFR scattering and impurity scattering. The role of IFR in low temperature luminescence has been analyzed in Refs. 11, 24, and 25.

As next we focus on the electron transport through LO-phonon emission, as this mechanism plays a protagonic role in low-temperature intersubband scattering for large ($E_{ij} > E_{\mathrm{LO}}$) intersubband energy spacings. According to Ref. 26, the correspondent scattering rate R_{ij}^{LO} can be calculated by

$$R_{ij}^{\mathrm{LO}} = \frac{1}{\tau_{ij}^{\mathrm{LO}}} = \frac{\int_0^\infty dk\, k f_i(k)/\tau_{ij}^{\mathrm{LO}}(k)}{\int_0^\infty dk\, k f_i(k)}, \tag{2}$$

where f_i denotes the Fermi-Dirac distribution of the *ith* subband. $(\tau_{ij}^{\mathrm{LO}}(k))^{-1}$ is the LO-phonon scattering rate of electrons from a state with momentum k in the initial *ith* subband to a state in the *jth* subband. This scattering rate is given by

$$\begin{aligned}\frac{1}{\tau_{ij}^{\mathrm{LO}}(k)} &= \pi Y'' \Theta\left(k^2 + \frac{2m^*\Delta_{ij}}{\hbar^2}\right) \int_0^\infty dK_z \\ &\times \frac{|G_{ij}(K_z)|^2}{\sqrt{K_z^4 + 2K_z^2\left(2k^2 + \frac{2m^*\Delta_{ij}}{\hbar^2}\right) + \left(\frac{2m^*\Delta_{ij}}{\hbar^2}\right)^2}} \\ &= \pi Y'' \Theta\left(k^2 + \frac{2m^*\Delta_{ij}}{\hbar^2}\right) \int_0^\infty dK_z\, F(K_z, k).\end{aligned} \tag{3}$$

Here, k denotes the in-plane electron wavevector and K_z the phonon wavevector perpendicular to the layer. Y'' describes the temperature dependence and Θ denotes the step function. $\Delta_{ij} = E_i - E_j \mp E_{\mathrm{LO}}$, where the minus sign refers to the LO phonon emission and the plus sign to the LO phonon absorption. At low temperatures, we neglect the LO phonon absorption, because the thermal population of the phonon modes is negligible. The modulus squared of the form factor $|G_{ij}(K_z)|^2 = \int dz dz' \psi_i(z)\psi_i^*(z') \exp[-iK_z(z-z')]\psi_j^*(z)\psi_j(z')$ restricts the probability of scattering in k space.

In general, the LO phonon scattering according to Eq. (3) cannot be completely described by a linear dependence on the wave function overlap ζ_{ij}. Nevertheless, such a linear dependence appears to be an appropriate approximation for many QCL structures. For a typical MIR QCL design,[27,28] Fig. 1(a) shows the calculated dependence of the modulus squared of the form factor $|G_{ij}(K_z)|^2$ for the main laser

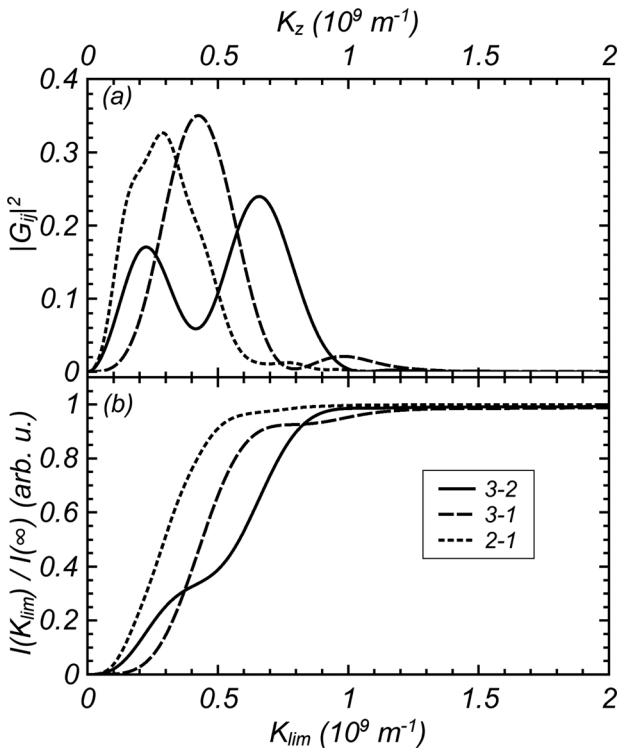

FIG. 1. (a) Form factor $|G_{ij}(K_z)|^2$ and (b) the ratio of integrals $I(K_{\mathrm{lim}})$ to $I(K_{\mathrm{lim}} = \infty)$ according to Eq. (4) for the indicated transitions for a typical MIR QCL design.[27]

transitions. For $K_z \gg 10^9\,\mathrm{m}^{-1}$, the form factor approaches zero. In Fig. 1(b), the expression

$$I(K_{\mathrm{lim}}) = \int_0^{K_{\mathrm{lim}}} dK_z F(K_z, 0) \tag{4}$$

is shown as a function of the upper limit K_{lim}. For $K_z > 10^9\,\mathrm{m}^{-1}$, $I(K_{\mathrm{lim}})$ saturates, implying that the main part of integral $\int_0^{\infty} dK_z F(K_z, 0)$ in Eq. (4) results from the integration over region $(0, K_{\mathrm{lim}})$. However, if $\Delta_{ij} \gg 0$, the expression $1/\sqrt{K_z^4 + 2K_z^2\left(2k^2 + \frac{2m^*\Delta_{ij}}{\hbar^2}\right) + \left(\frac{2m^*\Delta_{ij}}{\hbar^2}\right)^2}$ is practically constant for these K_z values. In this case, it can be taken out of the integral in Eq. (3). We then obtain

$$\frac{1}{\tau_{ij}^{\mathrm{LO}}(k)} = \pi Y'' \frac{\Theta\left(k^2 + \frac{2m^*\Delta_{ij}}{\hbar^2}\right) \int_0^{K_{\mathrm{lim}}} dK_z |G_{ij}(K_z)|^2}{\sqrt{K_{\mathrm{lim}}^4 + 2K_{\mathrm{lim}}^2\left(2k^2 + \frac{2m^*\Delta_{ij}}{\hbar^2}\right) + \left(\frac{2m^*\Delta_{ij}}{\hbar^2}\right)^2}}. \tag{5}$$

While the integrand $|G_{ij}(K_z)|^2$ tends to zero beyond K_{lim}, the upper limit of the integral can be extended to ∞. In this case,

$$\int_0^{K_{\mathrm{lim}}} dK_z |G_{ij}(K_z)|^2 \approx \int_0^{+\infty} dK_z |G_{ij}(K_z)|^2 = \pi\zeta_{ij}. \tag{6}$$

For energies higher than E_{LO}, the value of $k^2 + \frac{2m^*\Delta_{ij}}{\hbar^2}$ is always positive, and Eq. (5) becomes

$$\frac{1}{\tau_{ij}^{\mathrm{LO}}(k)} = \pi Y'' \frac{\pi\zeta_{ij}}{\sqrt{K_{\mathrm{lim}}^4 + 2K_{\mathrm{lim}}^2\left(2k^2 + \frac{2m^*\Delta_{ij}}{\hbar^2}\right) + \left(\frac{2m^*\Delta_{ij}}{\hbar^2}\right)^2}}. \tag{7}$$

If $m^*\Delta_{ij}/\hbar^2 \gg k^2$, Eq. (7) reduces to

$$\frac{1}{\tau_{ij}^{\mathrm{LO}}(0)} = \frac{\pi^2 Y''/K_{\mathrm{lim}}^2}{1 + \frac{2m^*}{\hbar^2 K_{\mathrm{lim}}^2}\Delta_{ij}}\zeta_{ij}. \tag{8}$$

Although the above derivation strictly holds only for $\Delta_{ij} \gg 0$, we approximate the LO phonon scattering by a linear dependence on the wave function overlap for the entire range of E_{ij} values. Because in the MIR region the scattering rate $(\tau_{ij}^{\mathrm{LO}}(k))^{-1}$ is practically independent of k, Eq. (2) becomes

$$R_{ij}^{\mathrm{LO}} = \frac{1}{\tau_{ij}^{\mathrm{LO}}(0)} = \frac{\rho^{\mathrm{LO}}(E_{\mathrm{LO}})}{1 + a(E_{ij} - E_{\mathrm{LO}})}\zeta_{ij} = \rho^{\mathrm{LO}}(E_{ij})\zeta_{ij}, \tag{9}$$

where $\rho^{\mathrm{LO}}(E_{\mathrm{LO}}) = \pi^2 Y''/K_{\mathrm{lim}}^2$, $a = 2m^*/(\hbar^2 K_{\mathrm{lim}}^2)$, and

$$\rho^{\mathrm{LO}}(E_{ij}) = \frac{\rho^{\mathrm{LO}}(E_{\mathrm{LO}})}{1 + a(E_{ij} - E_{\mathrm{LO}})}. \tag{10}$$

Using Eq. (2), we calculate the function $\rho^{\mathrm{LO}}(E_{ij}) = R_{ij}^{\mathrm{LO}}/\zeta_{ij}$ for 1 THz and two MIR QCL designs. Results are presented in Fig. 2. The dependence of ρ^{LO} on E_{ij} can be separated into two parts: one for energies below and one for energies above the LO phonon energy. The energy dependence of ρ^{LO} for $E < E_{\mathrm{LO}}$ can be described by a Fermi-Dirac distribution for $E_{ij} - E_{\mathrm{LO}}$, whereas for $E > E_{\mathrm{LO}}$ it can be approximated by $\rho^{\mathrm{LO}}(E_{ij})$ defined in Eq. (10).

In order to get the total non-radiative scattering rate, we integrate this function with the phenomenological formula given in Ref. 13. We do this by writing a single equation

$$R_{ij} = \begin{cases} \rho(E_{ij})\zeta_{ij} & \text{for} \quad E_{ij} \le E_{LO} \\ \dfrac{\rho(E_{ij})\zeta_{ij}}{1 + a(E_{ij} - E_{\mathrm{LO}})} & \text{for} \quad E_{ij} > E_{LO} \end{cases} \tag{11}$$

which consists of two parts: The low-energy ($E_{ij} < E_{\mathrm{LO}}$) part—described in detail in Appendix—has the functional of Ref. 13 and parametrizes contributions arising from several non-radiative scattering mechanisms including electron-electron and interface-roughness scattering. The high-energy ($E_{ij} > E_{\mathrm{LO}}$) part has the decay behavior with increasing intersubband energy spacing described by Eqs. (9) and (10).

Note that electron-LO-phonon emission describes the shape of the function R_{ij} for $E_{ij} > E_{\mathrm{LO}}$, yet it does not give the absolute values. In order to get the absolute non-radiative scattering rate values, we need to fit Eq. (11) to real QCL data using the fit parameter a. Doing this, we incorporate several non-radiative scattering mechanisms—among others interface roughness scattering—in our model, which were left out in our analysis of the scattering rate for $E_{ij} > E_{\mathrm{LO}}$. Finally, note that in contrast to Ref. 13, where the focus was on transitions with energies below or near the LO phonon energy, the wave function depending contribution is now the overlap ζ_{ij} rather than the dipole matrix element.

Using literature data for R_{ij} corresponding to different intersubband transitions in QCLs and calculating the corresponding exchange integrals ζ_{ij}, the prefactors of ζ_{ij} in Eq. (11) are reconstructed. The respective results are shown in Fig. 3 for the fit parameter $a = 0.0494\,\mathrm{meV}^{-1}$.

Using the coupled Schrödinger-Poison equations,[18] the full set of wave functions for the system under consideration is determined. Based on this, the charge distribution and current density can be obtained solving the full system of rate

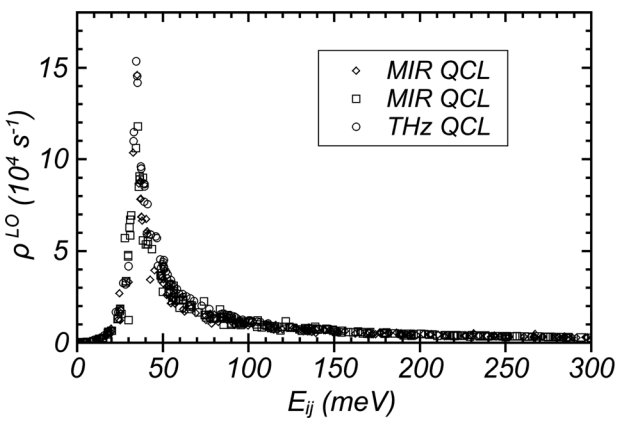

FIG. 2. The values of $\rho^{\mathrm{LO}}(E_{ij})$ as a function of E_{ij} for two typical MIR[27,28] and one THz (Ref. 29) QCL designs.

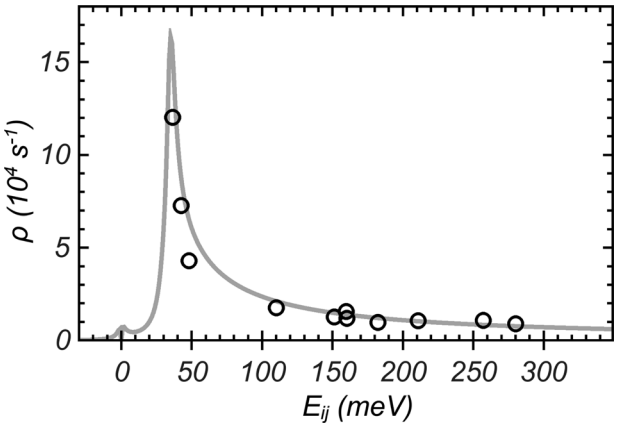

FIG. 3. Prefactors of ζ_{ij} in Eq. (11) as a function of the transition energy E_{ij} for QCLs based on (In,Ga)As/(In,Al)As heterostructures. The open symbols represent the values of R_{ij}/ζ_{ij} for various $In_{0.52}Al_{0.48}As/In_{0.53}Ga_{0.47}As$ samples reported in the literature.[27,28,30–34] The solid line is a fit to the data.

equations for $3N$ wave functions in three periods with N states in each period. This system has the form

$$\frac{dn_i}{dt} = \sum_{j=1}^{N} n_j \left[R^*_{ji} + R^*_{j+N,i} + R^*_{j-N,i}\right] - n_i \sum_{j=1}^{N} \left[R^*_{ij} + R^*_{i,j+N} + R^*_{i,j-N}\right], \quad (12)$$

where $R^*_{ij} = R_{ij} + R^{ph}_{ij}$ denotes the full scattering rate from the *ith* to the *jth* level, which includes non-radiative transitions R_{ij} [Eq. (11)] and radiative transitions R^{ph}_{ij}.[14,18] n_i denotes the electron sheet density in level i. Levels j, $j-N$, and $j+N$ are adjacent wave functions in the first, second, and third cascades, respectively. In Eq. (12), the first term of the sum collects scattering contributions populating the level i from the other $3N-1$ levels and the second term represents the contributions depopulating this level to the other $3N-1$ levels.

The current density is determined by

$$J = \sum_{i,j=1}^{N} n_i [\phi_{ij} R^*_{ij} - R^*_{i,j+N} + R^*_{i,j-N}] \quad (13)$$

with $\phi_{ij} = 1, -1$, or 0 for the transitions of electrons from left to right, from right to left, or far away from any virtual interface, respectively.

The proposed model is applied to the case of low temperature (<100 K) and low electron concentration ($<10^{18}\,cm^{-3}$) QCL. In this case, the leakage of carriers into continuum states can be neglected.[17]

III. SIMULATION RESULTS FOR AN MIR QCL

Let us apply the developed model to a broadband QCL at a low temperature (80 K). The QCL design is based on the $In_{0.52}Al_{0.48}As$-$In_{0.53}Ga_{0.47}As$ heterosystem with AlAs barriers in the active region to minimize the carrier leakage. The QCL band structure is shown for two different field strengths in Figs. 4(a) and 4(c). As a result of the self-consistent calculations using Eq. (12), we obtain the electron sheet densities n_i for the different electron subbands i as shown in Figs. 4(b) and 4(d).

For a comparison of the results of the simulations with experimental data, we have grown a 40-staged structure by gas-source molecular beam epitaxy, which has been processed into 25 μm-wide ridges using conventional optical lithography and wet chemical etching. A 0.5 μm-thick SiO_2 layer was deposited by reactive magnetron sputtering for electrical insulation of the sidewalls. Cr/Au contacts were evaporated for the top metallization. Laser chips with uncoated facets of several resonator lengths L were mounted epilayer upon Cu holders.

Figure 5 shows (asterisks) the typical optical power-current density J–P and electric field-current density J–V curves measured for a 25 μm-wide and 4.0 mm long device mounted in a liquid nitrogen cryostat and driven by 500 ns pulses with a duty cycle of 0.5% at heat sink temperature of 80 K. Dots represent J–P and J–V calculation results using Ref. 14 and Eq. (13), respectively. For the calculations, we

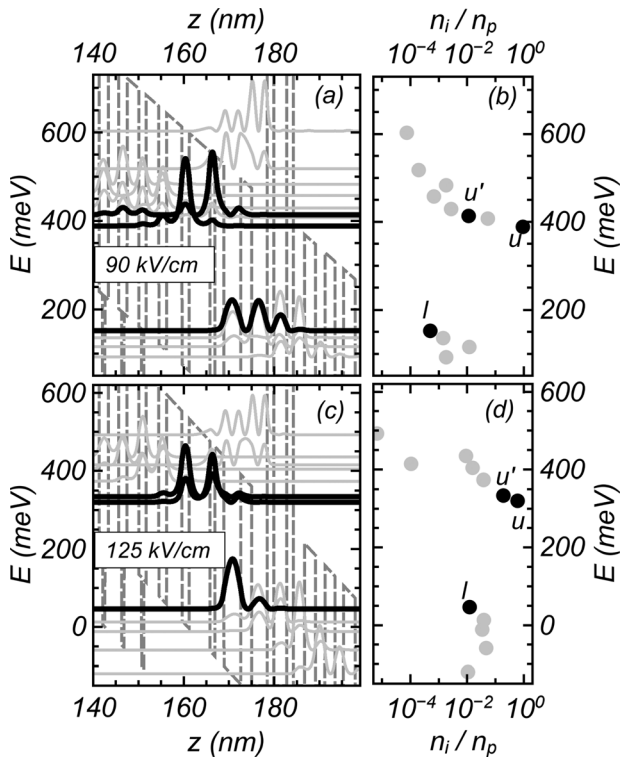

FIG. 4. (a) The conduction band profile of the investigated QCL for an applied electric field of 90 kV/cm at threshold and (c) for 125 kV/cm at the maximum of the emitted power. The layer thicknesses in nm from left to right starting from the widest active region quantum well are 3.4/*1.6*/4.6/*1.1*/2.0/*3.7*/2.4/*3.5*/**1.4**/*0.7*/***0.4***/*0.7*/***0.4***/*0.7*/**1.4**/*1.0*/***0.5***/*1.0*/2.4/*0.8*/***0.5***/*0.8*/2.2/*0.7*/***0.5***/*0.7*/2.6/*0.6*/***0.5***/*0.5*/2.8/*1.7*, where the $In_{0.52}Al_{0.48}As$ layers are denoted by regular, the $In_{0.53}Ga_{0.47}As$ layers by italic, the AlAs layers by bold, and the InAs layers by bold italic font. Underlined layers are n-doped resulting in a sheet density per period of $n_p = 2.5 \times 10^{11}\,cm^{-2}$. Only relevant Wannier-Stark levels are shown. u, u', and l are the moduli squared of the wave functions of the two upper laser levels and the lower laser level, respectively. (b) and (d) show the corresponding average two-dimensional sheet density n_i/n_p for the different levels resulting from self-consistent calculation of the rate equations for 90 kV/cm and 125 kV/cm, respectively. A heat sink temperature of 80 K is assumed.

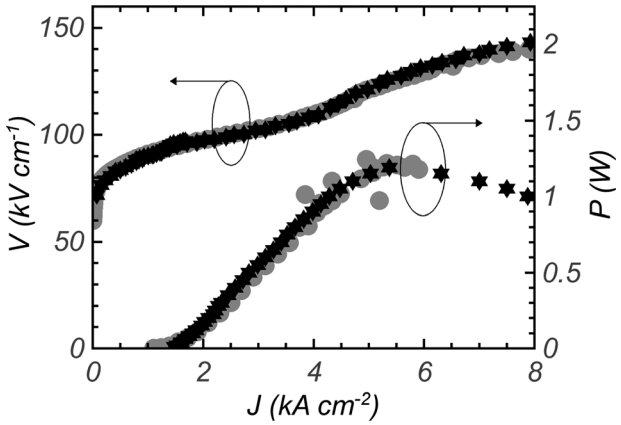

FIG. 5. Measured (asterisks) and calculated (dots) electric field-current density and optical power-current density characteristics for a $0.025 \times 4.0\,\mathrm{mm}^2$ device. The device was driven by 500 ns current pulses with a duty cycle of 0.5% at a heat sink temperature of 80 K.

used the following parameters: mirror losses $\alpha_m = 3\,\mathrm{cm}^{-1}$, waveguide losses $\alpha_w = 0.677\,\mathrm{cm}^{-1}$, and optical confinement factor $\Gamma = 0.7$. These parameters were determined by the finite element calculations for a $0.025 \times 4.0\,\mathrm{mm}^2$ device. Additional fitting parameters are the sheet-density per cascade $n_p = 2.5 \times 10^{11}\,\mathrm{cm}^{-2}$ and $2\gamma_0 = 2.5\,\mathrm{meV}$, where γ_0 is a correction parameter to accurately describe the spectral line shape $L_{ij}(\omega)$ (Ref. 14)

$$L_{ij}(\omega) = \frac{1}{\pi}\frac{\gamma_b}{(\gamma_b/2)^2 + (\hbar\omega - Eij)^2}\ . \tag{14}$$

$\gamma_b = \hbar(R_i + R_j) + 2\gamma_0$ describes here the total transition broadening and R_i (R_j) is the reciprocal lifetime for level i (j). The correction factor γ_0 can be found from electro luminescence data[24,35] or, as in this work, used as a fitting parameter in order to integrate scattering processes that are not included in Eq. (11) into calculations.

Calculated J–V characteristics are in good agreement with the measured data. The observed weak "kink" around $4\,\mathrm{kA\ cm}^{-2}$ is related to the particular wave function alignment around 115 kV cm^{-2} (just before roll-over), which results in a resonance between levels u and u'. Due to a numerical effect, the calculated optical power–current density characteristic becomes noisy after the laser roll-over (maximum of emitted power) and is omitted in Fig. 5. It is important to point out that using a rate equation approach might lead to non-physical effects as resonances in the J–V line (see, for example, Ref. 13). Despite the danger of such spurious features showing up, we do not observe such effects in the investigated voltage range (50–150 kV/cm).

Measured laser spectra and calculated photon flux spectra for different voltage (current density) values are presented in Fig. 6. Both the calculated and measured spectra show the same spectral position and the same broadening trend toward higher energies. The observed broadening is related to the increased population of upper laser levels with increased current. The observed blue-shift in the photon energy is related to the intersubband spacing increase between the upper laser states and the lower laser state characteristic for diagonal-transition QCLs.[9]

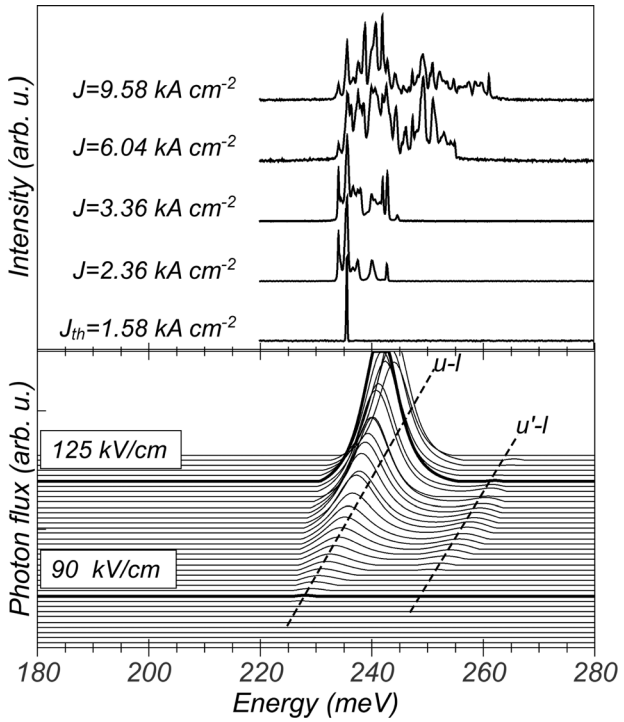

FIG. 6. Emission spectrum for a $0.025 \times 4.0\,\mathrm{mm}^2$ device of the investigated QCL collected with a high-resolution Fourier-transform spectrometer. The heat sink temperature is 80 K, and the injected current density is varied as indicated. The corresponding calculated spectra as a function of voltage are shown in the lower panel with the broadening parameter $2\gamma_0 = 2.5\,\mathrm{meV}$. Dashed lines indicate the transitions between the upper laser levels u as well as u' and the lower laser level l. Thick solid lines denote the threshold voltage of 90 kV/cm and the voltage with maximum power emitting at 125 kV/cm.

IV. CONCLUSIONS

A phenomenological model accounting for different scattering mechanisms has been developed for the simulations of both MIR and THz QCLs. The model uses scattering rates in the form of the product of an energy-dependent factor and the wave function overlap, which subsumes several non-radiative scattering processes in QCLs. The approach developed in this work was applied to a broad-band MIR QCL operated in pulsed mode with a low duty cycle and a heat sink temperature of 80 K. First results show a satisfactory agreement between the calculated and measured laser characteristics.

ACKNOWLEDGMENTS

The authors acknowledge the support in part by the German Research Foundation (DFG) and the European Union through the Erasmus Mundus External Cooperation Window program.

APPENDIX: SCATTERING RATE PARAMETRIZATION

The energy-dependent factor $\rho(E_{ij})$, which subsumes all non-radiative scattering processes in QCLs, is described by the empirical expression in Ref. 13

$$\rho(E_{ij}) = \frac{\rho_0(E_{ij})}{2}\left[\exp(A_1)[1-\Phi(A_2)] + 1 + \Phi(A_3)\right] \times \left[1 + k_{\mathrm{LO}}\left(1 + \Phi(A_4) + E_0\frac{\Gamma}{(E_{ij}-E_{\mathrm{LO}})^2+\Gamma^2}\right)\right], \tag{A1}$$

where

$$A_1 = \frac{E_{ij}}{E_a} + \frac{\sigma^2}{2E_a}, \quad A_2 = \frac{E_{ij}}{\sqrt{2}\sigma} + \frac{\sigma^2}{\sqrt{2}E_a^2}, \quad A_3 = \frac{E_{ij}}{\sqrt{2}\sigma}, \quad A_4 = \frac{E_{ij}-E_{\mathrm{LO}}}{\sigma_s}. \tag{A2}$$

and

$$\rho_0(E_{ij}) = \frac{2000|E_{ij}|}{E_{\mathrm{LO}}}\left(1 + \frac{aE_{\mathrm{LO}}}{bE_{ij}^2 + cE_{\mathrm{LO}}} - \frac{a}{bE_{\mathrm{LO}}+c}\right)c^{-1}. \tag{A3}$$

The parameters $E_a = 10.0\,\mathrm{meV}$, $\sigma = 5.0\,\mathrm{meV}$, $\Gamma = 5.0\,\mathrm{meV}$, and $E_0 = 10.0\,\mathrm{meV}$ describe thermal activation, interface roughness, broadening, and strength of the LO phonon resonance, respectively. Furthermore, $\sigma_s = 2.0\,\mathrm{meV}$ and $k_{\mathrm{LO}} = 25.0$ denote the width and magnitude of the step-like increase of $\rho(E_{ij})$ at the LO phonon resonance, respectively. $\Phi(x)$ denotes the error function. The parameters $a = 10$, $b = 2\,\mathrm{meV}^{-1}$, and $c = 0.1$ with a correction factor of $2000\,\mathrm{c}^{-1}$ lead to the scattering rates similar to the ones in (In,Ga)As/(In,Al)As QCLs. The scaling factor $\rho_0(E_{ij})$ in the approximation of Ref. 13 is constant and equals to $\rho_0(E_{\mathrm{LO}})$ for the region of energies higher than E_{LO}. In our consideration, this factor $\rho_0(E_{ij})$ is energy dependent and takes the form of Eq. (11).

[1]J. Faist, F. Capasso, D. L. Sivco, C. Sirtori, A. L. Hutchinson, and A. Y. Cho, Science **264**, 553 (1994).
[2]Y. Yao, A. J. Hoffman, and C. F. Gmachl, Nat. Photonics **6**, 432 (2012).
[3]S. Slivken, A. Evans, W. Zhang, and M. Razeghi, Appl. Phys. Lett. **90**, 151115 (2007).
[4]M. Razeghi, S. Slivken, Y. Bai, B. Gokden, and S. R. Darvish, New J. Phys. **11**, 125017 (2009).
[5]J. D. Kirch, C.-C. Chang, C. Boyle, L. J. Mawst, D. Lindberg III, T. Earles, and D. Botez, Appl. Phys. Lett. **106**, 151106 (2015).
[6]J. Faist, C. Gmachl, F. Capasso, C. Sirtori, D. L. Sivco, J. N. Baillargeon, and A. Y. Cho, Appl. Phys. Lett. **70**, 2670 (1997).
[7]N. Yu, R. Blanchard, J. Fan, F. Capasso, T. Edamura, M. Yamanishi, and H. Kan, Appl. Phys. Lett. **93**, 181101 (2008).
[8]J. Faist, F. Capasso, D. L. Sivco, A. L. Hutchinson, C. Sirtori, and A. Y. Cho, Infrared Phys. Technol. **36**, 99 (1995).
[9]C. Gmachl, F. Capasso, D. L. Sivco, and A. Y. Cho, Rep. Prog. Phys. **64**, 1533 (2001).
[10]A. Wacker, Phys. Rev. B **66**, 085326 (2002).
[11]S.-C. Lee and A. Wacker, Phys. Rev. B **66**, 245314 (2002).
[12]R. C. Iotti and F. Rossi, Phys. Rev. Lett. **87**, 146603 (2001).
[13]L. Schrottke, M. Giehler, M. Wienold, R. Hey, and H. T. Grahn, Semicond. Sci. Technol. **25**, 045025 (2010).
[14]L. Schrottke, M. Wienold, M. Giehler, R. Hey, and H. T. Grahn, J. Appl. Phys. **108**, 103108 (2010).
[15]D. Botez, S. Kumar, J. C. Shin, L. J. Mawst, I. Vurgaftman, and J. R. Meyer, Appl. Phys. Lett. **97**, 071101 (2010).
[16]Y. Flores, M. P. Semtsiv, M. Elagin, G. Monastyrskyi, S. Kurlov, A. Aleksandrova, J. Kischkat, and W. T. Masselink, J. Appl. Phys. **113**, 134506 (2013).
[17]D. Botez, C.-C. Chang, and L. J. Mawst, J. Phys. D: Appl. Phys. **49**, 043001 (2016).
[18]C. Jirauschek and T. Kubis, Appl. Phys. Rev. **1**, 011307 (2014).
[19]K. Donovan, P. Harrison, and R. W. Kelsall, J. Appl. Phys. **89**, 3084 (2001).
[20]W. A. Harrison, Phys. Rev. **104**, 1281 (1956).
[21]C. Y. Chang and F. Kai, *GaAs High-Speed Devices* (Wiley, New York, 1994).
[22]A. Vasanelli, A. Leuliet, C. Sirtori, A. Wade, G. Fedorov, D. Smirnov, G. Bastard, B. Vinter, M. Giovannini, and J. Faist, Appl. Phys. Lett. **89**, 172120 (2006).
[23]R. Nelander and A. Wacker, Appl. Phys. Lett. **92**, 081102 (2008).
[24]J. B. Khurgin, Y. Dikmelik, P. Q. Liu, A. J. Hoffman, M. D. Escarra, K. J. Franz, and C. F. Gmachl, Appl. Phys. Lett. **94**, 091101 (2009).
[25]A. Y. Song, R. Bhat, P. Bouzi, C.-E. Zah, and C. F. Gmachl, e-print arXiv:1507.06016.
[26]P. Harrison, *Quantum Wells, Wires and Dots*, 3rd ed. (Wiley, Chichester, 2009).
[27]C. Sirtori, J. Faist, F. Capasso, D. L. Sivco, A. L. Hutchinson, S. N. G. Chu, and A. Y. Cho, Appl. Phys. Lett. **68**, 1745 (1996).
[28]C. Sirtori, J. Faist, F. Capasso, D. L. Sivco, A. L. Hutchinson, and A. Y. Cho, Appl. Phys. Lett. **69**, 2810 (1996).
[29]M. Fischer, G. Scalari, K. Celebi, M. Amanti, Ch. Walther, M. Beck, and J. Faist, Appl. Phys. Lett. **97**, 221114 (2010).
[30]C. Sirtori, J. Faist, F. Capasso, D. L. Sivco, A. L. Hutchinson, and A. Y. Cho, Appl. Phys. Lett. **66**, 3242 (1995).
[31]J. Faist, F. Capasso, C. Sirtori, D. L. Sivco, J. N. Baillargeon, A. L. Hutchinson, S.-N. G. Chu, and A. Y. Cho, Appl. Phys. Lett. **68**, 3680 (1996).
[32]C. Gmachl, F. Capasso, J. Faist, A. L. Hutchinson, A. Tredicucci, D. L. Sivco, J. N. Baillargeon, S. N. G. Chu, and A. Y. Cho, Appl. Phys. Lett. **72**, 1430 (1998).
[33]C. Gmachl, A. Tredicucci, F. Capasso, A. L. Hutchinson, D. L. Sivco, J. N. Baillargeon, and A. Y. Cho, Appl. Phys. Lett. **72**, 3130 (1998).
[34]C. Gmachl, F. Capasso, A. Tredicucci, D. L. Sivco, A. L. Hutchinson, S. N. G. Chu, and A. Y. Cho, Appl. Phys. Lett. **73**, 3830 (1998).
[35]A. Wittmann, Y. Bonetti, J. Faist, E. Gini, and M. Giovannini, Appl. Phys. Lett. **93**, 141103 (2008).